Chinese Journal of Structural Chemistry

ARTICLE

Highly Efficient Photocatalytic CO_2 Methanation over Ru-Doped TiO_2 with Tunable Oxygen Vacancies

Zheyue Li[1†], Di Wu[1†], Wanbing Gong[1*], Jiayi Li[1], Shuaikang Sang[1], Hengjie Liu[1], Ran Long[1] and Yujie Xiong[1,2*]

[1]*Hefei National Research Center for Physical Sciences at the Microscale, School of Chemistry and Materials Science, National Synchrotron Radiation Laboratory, School of Nuclear Science and Technology, University of Science and Technology of China, Hefei 230026, China*

[2]*Institute of Energy, Hefei Comprehensive National Science Center, 350 Shushanhu Rd., Hefei 230031, China*

ABSTRACT Solar-driven CO_2 methanation is an imperative and promising approach to relieve the global warming and environmental crisis, yet remains a great challenge due to the low reaction efficiency, unsatisfactory selectivity and poor stability. In this work, we demonstrate a facile and efficient strategy to prepare Ru-doped TiO_2 photocatalyst with tunable oxygen vacancies using the ascorbic acid as a reducing agent for the CO_2 methanation reaction. The optimal Ru-TiO_2-OV-50 exhibits a remarkable CH_4 production rate of 81.7 mmol g^{-1} h^{-1} with a 100% CH_4 selectivity under a 1.5 W cm^{-2} light illumination, which is significantly higher than commercial Ru/TiO_2 and other reported catalysts. We reveal that the superior photocatalytic CO_2 methanation performance is mainly due to the synergistic effect of Ru doping and TiO_2 with tunable oxygen vacancies. Impressively, the light rather than thermal effect is confirmed as the main influencing factor by experimental studies. In addition, *in situ* spectroscopic technology is performed to investigate the CO_2 methanation reaction pathway. This work will open an avenue to design and prepare highly efficient photocatalyst with tunable oxygen vacancies for CO_2 conversion and other related applications.

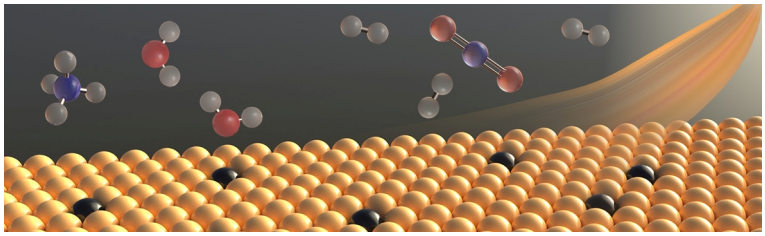

Keywords: photocatalysis, CO_2 methanation, metal doping, titanium oxide, oxygen vacancies

n INTRODUCTION

The chemical conversion of carbon dioxide (CO_2) and hydrogen (H_2) into downstream fuels and chemicals is regarded as an efficient and promising technology to reduce atmospheric CO_2 concentration and thus reliance on fossil resources.[1-3] Among them, the CO_2 hydrogenation to high energy methane (CH_4), *i.e.*, the Sabatier reaction has great potential in modern chemical industries.[4,5] For instance, Guo *et al.* revealed the outstanding thermocatalytic CO_2 hydrogenation activity and 98-100% CH_4 selectivity can be obtained on the Ru nanoclusters/CeO_2 catalyst, but the reaction temperature was still up to 190 °C.[6] In this regard, the photocatalytic CO_2 methanation using renewable solar energy has emerged as one of the most promising and green routes, yet remains a significant challenge because of the unsatisfactory reaction efficiency and CH_4 selectivity.[7-12] Meanwhile, the design and development of high-efficient photocatalyst is urgently needed to overcome key problems such as thermodynamically inertia of CO_2, slow kinetic process limitation and low light utilization efficiency.[13,14] So far, considerable progress has been made to develop CO_2 methanation semiconductor photocatalysts,[15,16] including CeO_2-,[17] TiO_2-,[18] $SrTiO_3$-,[19] and $Ni_2V_2O_7$-[8] based catalysts. Although great progress has been made, the fabrication of highly active, selective and stable photocatalyst is still in urgent requirement for CO_2 methanation under mild conditions.[20]

Among these semiconductor photocatalysts, TiO_2-based catalysts have been intensively investigated due to their low cost, simple synthesis and chemical stability for the energy and environmental applications. However, the photocatalytic performance of reported TiO_2-based catalysts can not meet specific requirements for the CO_2 methanation because of their limited charge separation efficiency and low CO_2 activation capabilities.[18,21] Fortunately, many strategies have been recently proposed to improve photocatalytic performance of TiO_2-based catalysts such as heterojunction construction,[22,23] heteroatom doping,[24] metal cocatalyst[25-28] and defect engineering.[29-31] Considering the requirement for activating CO_2 and H_2, the construction of metal cocatalyst is an ideal strategy over the TiO_2-based materials to improve the photocatalytic CO_2 methanation by simultaneously promoting the charge separation and reactant activation. Among various metals that have been explored, Ru site has been considered as a promising candidate for low temperature CO_2 methanation reactions.[8,32,33] For instance, Ye's group demonstrated Ru possessed an efficient ability to promote the photogenerated charge separation as well as the hydrogen activation and utilization for the CO_2 photo-hydrogenation to CH_4.[34] Besides, Cai *et al.* recently have showed the introduction of Ru species on CdS greatly promoted the activation of CO_2 and the separation efficiency of photogenerated carriers, thus accelerating the conversion of CO_2 to CH_4.[35] Based on the above considerations, the Ru-TiO_2 composite can be further used to improve photocatalytic CO_2 methanation performance, yet has rarely been reported. In this respect, Zhou *et al.* reported the 1% Ru-TiO_{2-x} nanocrystal with abundant oxygen vacancies exhibited a remarkable photocatalytic performance with a CH_4 yield of 31.63 μmol g^{-1} h^{-1} due to synergistic effect of Ru and oxygen

DOI: 10.14102/j.cnki.0254-5861.2022-0212

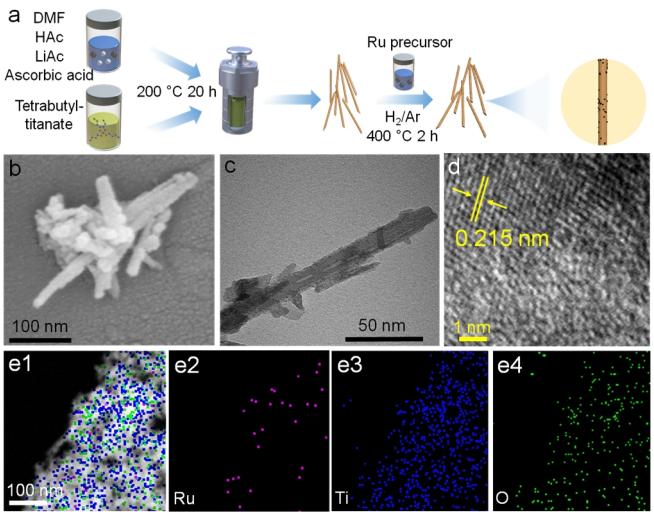

Figure 1. (a) Schematic illustration of the synthesis of Ru/TiO_2-OV-x catalysts. (b) SEM image, (c) TEM image, (d) HRTEM image and (e) TEM element mapping images of Ru/TiO_2-OV-50 catalyst.

vacancies.[21] Lin *et al.* reported that the Ru/$TiO_{(2-x)}N_x$ catalyst exhibited superior light-assisted CO_2 methanation performance, which was resulted from the combined effect of oxygen vacancies and electron-rich Ru sites.[18] Therefore, it is highly desirable to prepare Ru-TiO_2 photocatalyst to catalyze CO_2 methanation process, which can effectively improve the charge separation and reactant activation due to the synergistic effect of Ru and TiO_2 with oxygen vacancies.

In this work, we report a facile and efficient strategy to synthesize Ru-doped TiO_2 with abundant oxygen vacancies by using ascorbic acid as a reducing agent. The as-synthesized Ru/TiO_2-OV-50 catalyst exhibits an outstanding activity, selectivity and stability for the photocatalytic hydrogenation of CO_2 to CH_4 with an 81.7 mmol·g^{-1}·h^{-1} reaction rate and 100% CH_4 selectivity at a 1.5 W·cm^{-2} light illumination. The experimental results show the enhanced photocatalytic CO_2 methanation performance is due to the synergistic effect of Ru and TiO_2 with tunable oxygen vacancies, which is mainly resulted from the light rather than the thermal effect. Finally, the CO_2 methanation reaction pathway on this catalyst is also proposed using *in situ* spectroscopic technology.

n RESULTS AND DISCUSSION

The synthetic process of Ru/TiO_2-OV-x (x stands for the ascorbic acid amount) is schematically illustrated in Figure 1a. Briefly, the TiO_2-OV-x precursors with tunable oxygen vacancies were first synthesized by a simple solvothermal method using ascorbic acid as a reducing agent. The as-synthesized TiO_2-OV-x precursors exhibit rod-like shape from the transmission electron microscopy (TEM) images (Figure S1). Notably, the TiO_2-OV-x nanorods become shorter in length and larger in diameter with the increase of ascorbic acid amount. Subsequently, an electrostatic adsorption-reduction strategy was used to prepare Ru/TiO_2-OV-x, which was finally reduced at 400 ºC for 2 h under a 10 vol% H_2/Ar flow. The scanning electron microscopy (SEM) and TEM images (Figures S2, 3) show that the original morphology of TiO_2-OV-x precursors is preserved well after the introduction of Ru species. For the typical Ru/TiO_2-OV-50 catalyst, the rod-like shape with around 100-200 nm in length and 10-20 nm in diameter is well maintained after the reduction treatment (Figure 1b, c). High-resolution TEM (HRTEM) image (Figure 1d) shows a lattice spacing of 0.215 nm corresponding to the (002) lattice fringe of metallic Ru. The average size of Ru sites is around 2-3 nm (Figure S4). The corresponding TEM elemental mapping images (Figure 1e) reveal highly homogeneous distributions of Ru, Ti and O over the skeleton. For comparison, the Ru-doped commercial TiO_2 nanoparticles (NPs) catalyst (denoted as Ru/TiO_2) was also prepared using the same procedure, and the morphology and structure are shown in Figures S1f, 2f and 3f.

X-ray diffraction (XRD) patterns (Figure 2a) of Ru/TiO_2-OV-x show the anatase and rutile mixed phase TiO_2, which are different from the anatase phase of commercial TiO_2 (Figure S5). Impressively, characteristic XRD peaks of Ru species are not clearly observed after Ru doping, indicating the high dispersion of Ru species (Figures 2a, S6). X-ray photoelectron spectroscopy (XPS) was performed to investigate the surface properties and chemical states of the catalysts. As shown in Figure S7, the XPS survey spectra of Ru/TiO_2-OV-x show the presence of Ru, Ti and O elements. The Ru 3d spectra (Figure 2b) of Ru/TiO_2-OV-x at ~280.4 and 284.5 eV, which are assigned to $3d_{5/2}$ and $3d_{3/2}$ of Ru^0, respectively, indicating the transformation of Ru^{3+} into a lower valence state of Ru.[36] As the ascorbic acid amount increases, a shift to lower binding energy is observed. Such a negative shift indicates a higher electron density of Ru site, thus leading to a stronger ability to attach and activate CO_2.[37,38] The Ti 2p spectra (Figure S8) show the peaks at ~458 and 464 eV corresponding to Ti $2p_{3/2}$ and Ti $2p_{1/2}$, respectively.[38] Notably, a negative shift in the binding energy is observed with the increase of ascorbic acid amount, which indicates the more oxygen vacancies are generated on the surface of catalyst.[39] For the O 1s spectra (Figure S9), the peaks at 529.4 and 531.0 eV correspond to lattice oxygen species and adsorbed oxygen species, respectively.[40-42] Furthermore, the electron paramagnetic resonance (EPR) was employed to investigate the oxygen vacancies, and the results in Figure 2c exhibit an obvious signal at g = 2.003 for the Ru/TiO_2-OV-x catalysts, which is attributed to the oxygen vacancy signal.[43-46] It can be found that much higher intensity compared with Ru/TiO_2 and Ru/TiO_2-OV-0 confirmed the presence of abundant oxygen vacancies, which suggests the importance of ascorbic acid.[43] In addition, the contents of oxygen vacancies are accordingly increased after Ru doping due to the reductive treatment of H_2. The fine structure information of optimum Ru/TiO_2-OV-50 catalyst was further studied by X-ray absorption near-edge structure (XANES) and extended X-ray absorption fine structure (EXAFS) measurements. The white-line intensity of Ru/TiO_2-OV-50 is higher than that of Ru foil and lower than that of RuO_2, indicating a partial positive charge of Ru species (Figure 2d).[47] The corresponding Fourier transform EXAFS spectrum (Figure 2e) of Ru/TiO_2-OV-50 shows two obvious peaks at ~1.5 and 2.4 Å, which can be assigned to Ru-O and Ru-Ru

DOI: 10.14102/j.cnki.0254-5861.2022-0212

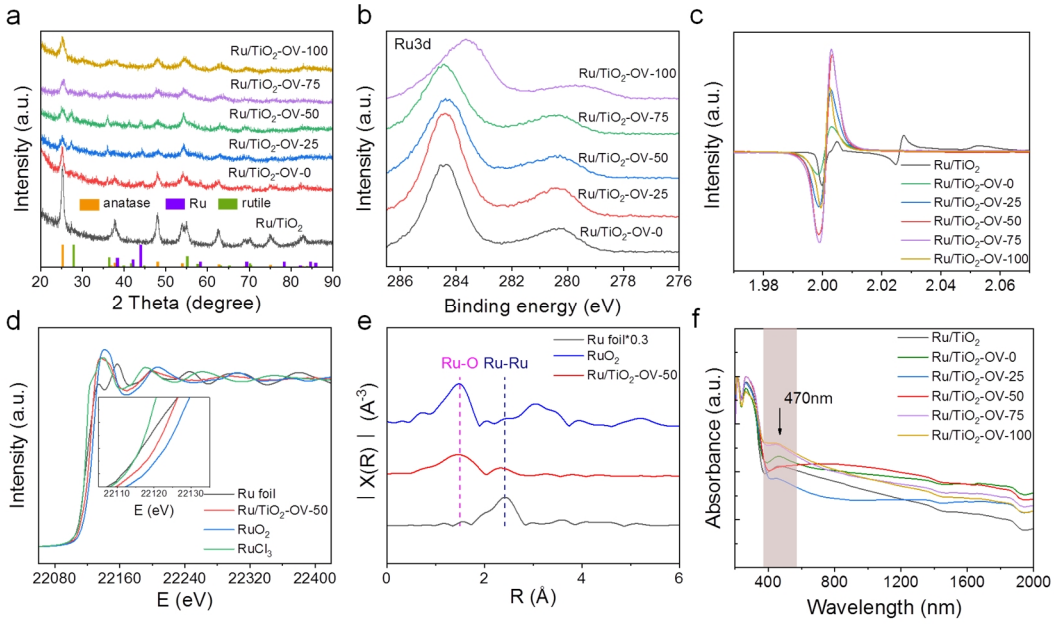

Figure 2. (a) XRD patterns and (b) high-resolution Ru 3d XPS spectra of Ru/TiO_2-OV-x catalysts. (c) EPR spectra of Ru/TiO_2 and Ru/TiO_2-OV-x catalysts. (d) XANES spectra and (e) EXAFS spectra of Ru foil, RuO_2 and Ru/TiO_2-OV-50 catalysts. (f) UV-vis-IR spectra of Ru/TiO_2 and Ru/TiO_2-OV-x catalysts.

coordination, respectively. According to the fitting results (Table S1), the coordination numbers of Ru-O and Ru-Ru are 1.41 and 3.95, respectively, which suggests the formation of low-coordination Ru clusters and NPs. The ultraviolet-visible-near infrared (UV-vis-IR) spectroscopy was used to investigate the light adsorption ability. Figure 2f shows the Ru/TiO_2-OV-x samples can adsorb visible-near infrared light with a range of 400-2000 nm, and an adsorption peak at λ = 470 nm corresponds to the interband adsorption of Ru species. Compared with the absorption spectra of TiO_2-OV-x samples (Figure S10), such excellent light absorption ability makes these candidates very suitable for photocatalytic CO_2 hydrogenation reaction. The Ru contents are respectively determined to be 1.8, 1.4, 1.5, 1.6, 1.9 and 2.1 wt.% for Ru/TiO_2, Ru/TiO_2-OV-0, Ru/TiO_2-OV-25, Ru/TiO_2-OV-50, Ru/TiO_2-OV-75 and Ru/TiO_2-OV-100 catalysts by inductively coupled plasma-atomic emission spectrometry (ICP-AES) analysis, which indicates that the loading amount of Ru sites increases with the increase of oxygen vacancies. Furthermore, the specific surface area measurements at 77 K (Figures S11, 12) show that the Ru/TiO_2-OV-50 gives a large specific surface area (152.0 m^2/g), which is about 1.5 and 1.8 times higher than those of Ru/TiO_2 (101.7 m^2/g) and Ru-TiO_2-OV-0 (83.6 m^2/g), respectively. It can be found that the specific surface area increases first and then decreases with the increase of ascorbic acid amount. In a word, the Ru-doped TiO_2 nanorods catalyst with tunable oxygen vacancies is successfully synthesized.

The photocatalytic CO_2 hydrogenation to CH_4 was used as a model reaction to evaluate the catalytic performance of as-synthesized samples. As seen in Figure 3a, the Ru/TiO_2-R catalyst shows a higher reaction rate (11.20 mmol·g^{-1}·h^{-1}) than Ru/TiO_2-A (0.43 mmol·g^{-1}·h^{-1}), Ru/CeO_2 (1.11 mmol·g^{-1}·h^{-1}), Ru/In_2O_3 (1.96 mmol·g^{-1}·h^{-1}) and Pd/TiO_2 (2.62 μmol·g^{-1}·h^{-1}) at an irradiation intensity of 1.0 W·cm^{-2}, which confirms the synergistic effect of Ru and TiO_2 for the enhanced photocatalytic CO_2 methanation performance. More importantly, an almost 100% CH_4 selectivity is obtained on the Ru/TiO_2 catalyst. Although it exhibits an excellent CH_4 selectivity, low reaction rate still needs to be improved due to the absence of oxygen vacancies over commercial TiO_2. For this purpose, a series of Ru/TiO_2-OV-x catalysts with tunable oxygen vacancies were synthesized. The results in Figure 3b show that Ru/TiO_2-OV-50 has an 81.7 mmol·g^{-1}·h^{-1} reaction rate with a 100% CH_4 selectivity, which is ~ 2.4 times higher than those of Ru/TiO_2 (34.6 mmol·g^{-1}·h^{-1}) and Ru/TiO_2-OV-0 (34.8 mmol·g^{-1}·h^{-1}) at an irradiation intensity of 1.5 W·cm^{-2}. This indicates the oxygen vacancies of TiO_2 nanorods can efficiently catalyze the photocatalytic CO_2 methanation reaction due to the generated active sites and better light response ability. In addition, the reaction rate increases first then decreases with the increase of ascorbic acid amount, suggesting the importance of tunable oxygen vacancies amount.

To optimize the reaction conditions and investigate the catalytic mechanism, a series of photocatalytic CO_2 methanation reactions were conducted over the optimum Ru/TiO_2-OV-50 catalyst. First, the influence of light intensity on catalytic performance was investigated. As shown in Figure 3c, no activity is observed in the absence of light irradiation, indicating the significance of light. The reaction rate is increased from 0.18 mmol·g^{-1}·h^{-1} at 0.4 W·cm^{-2} to 45.6 mmol·g^{-1}·h^{-1} at 1.2 W·cm^{-2}, and then the reaction rate is further increased to 81.7 mmol·g^{-1}·h^{-1} at 1.5 W·cm^{-2}. It is worth noting that the catalyst not only possesses excellent catalytic activity, but also displays 100% CH_4 selectivity. Considering the intensity distribution of the light at different frequencies, the apparent quantum efficiency is estimated to be 3.01% over Ru/TiO_2-OV-50 under the optimum reaction conditions.

DOI: 10.14102/j.cnki.0254-5861.2022-0212

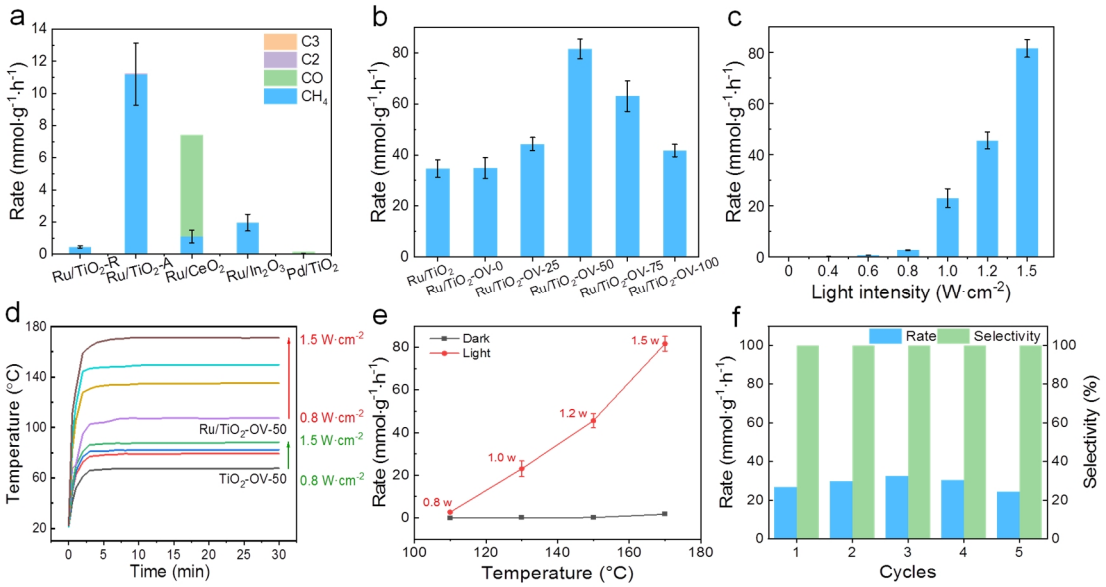

Figure 3. (a) Photocatalytic CO_2 methanation over different catalysts at an irradiation intensity of 1.0 W·cm^{-2} (Ru/TiO_2-R: rutile; Ru/TiO_2-A: anatase). (b) Photocatalytic CO_2 methanation over Ru/TiO_2 and Ru/TiO_2-OV-x catalysts at an irradiation intensity of 1.5 W·cm^{-2}. (c) Photocatalytic CO_2 methanation over Ru/TiO_2-OV-50 catalyst under different light intensities. (d) The photothermal temperature monitoring for the TiO_2-OV-50 and Ru/TiO_2-OV-50 catalysts. (e) The CO_2 methanation over Ru/TiO_2-OV-50 catalyst with and without light. (f) Stability test for photocatalytic CO_2 methanation over Ru/TiO_2-OV-50 catalyst under 1.0 W·cm^{-2}.

Compared to reported results (Table S2), our catalytic performance exceeds most of the reported metal catalysts. Herein, the photothermal effect towards the gas-phase CO_2 methanation reaction needs to be considered. Therefore, we monitored the surface temperature of the catalysts over time under light irradiation. The results show that the surface temperatures are rapidly increased in three to five minutes and then remain unchanged over the as-synthesized samples (Figures 3d, S13). Specifically, the surface temperatures over TiO_2-OV-50 sample are 67.7, 79.2, 82.3 and 88.2 °C at 0.8, 1.0, 1.2 and 1.5 W·cm^{-2}, respectively, which are much higher than those over commercial TiO_2 and TiO_2-OV-0 (Figure S13). It illustrates that the surface photothermal temperatures can be obviously increased in the presence of oxygen vacancies for the TiO_2 catalysts. After Ru doping, the surface temperatures are further increased due to the excellent optical adsorption properties of Ru site. For instance, the surface temperatures over Ru/TiO_2-OV-50 sample are 107.5, 135.1, 149.8 and 171.2 °C at 0.8, 1.0, 1.2 and 1.5 W·cm^{-2} (Figure 3d) respectively, indicating the excellent photothermal properties of metallic Ru site. To evaluate the contribution of thermal effect, we compared the catalytic performance with or without light irradiation. The results in Figure 3e reveal the reaction rates are 2.7, 23.0, 45.6 and 81.7 mmol·g^{-1}·h^{-1} at 0.8, 1.0, 1.2 and 1.5 W cm^{-2}, respectively, which are 82.3, 303.6, 263.4 and 48.1 times higher than those at the same reaction temperature under dark conditions, which confirm the significance of light other than thermal effect. In addition, we also explored the influence of wavelength on the catalytic performance of Ru/TiO_2-OV-50. As shown in Tables S3, 4, the ultraviolet light gives almost no contribution to catalytic performance. The visible light, especially the wavelength between 420-600 nm, plays the most important role for this catalytic reaction. Subsequently, the effect of mixed gas ratio on catalytic activity was investigated, as shown in Figure S14. The reaction rate and CH_4 selectivity increase with the increase of H_2 to CO_2 ratio, and a 100% CH_4 selectivity is obtained when the H_2 to CO_2 ratio is greater than 1. When H_2 to CO_2 ratio is less than 1, the main product is CO. At last, the cycling test was examined at an irradiation intensity of 1.0 W·cm^{-2}. The results in Figure 3f show the catalyst exhibits an excellent stability during five successive cycles. The XRD patterns of Ru/TiO_2-OV-50 before and after 5 cycles are almost the same (Figure S15), implying its structural stability.

To confirm the carbon source of the produced CH_4, isotope labelling experiment was carried out using $^{13}CO_2$ as reactant for CO_2 hydrogenation. The gas chromatography-mass spectroscopy (GC-MS) analysis (Figure S16) clearly confirms the origin of produced CH_4. Meanwhile, the high CH_4 selectivity is also confirmed by this isotope labelling experiment. Afterwards, the photocurrent and electrochemical impedance spectroscopy (EIS) results (Figure S17) show that the Ru/TiO_2-OV-50 has a higher photocurrent density and smaller arc radius than commercial Ru/TiO_2 and TiO_2-OV-50 samples, which suggests a higher charge separation efficiency and lower charge-transfer resistance over Ru/TiO_2-OV-50. Therefore, these results indicate the synergistic effect of Ru and TiO_2 with the oxygen vacancies for the enhanced photocatalytic CO_2 methanation performance. As for the role of oxygen vacancies, the transfer of photoexcited electrons TiO_2 with oxygen vacancies to the electron-rich Ru NPs promotes the adsorption and dissociation of CO_2 on the Ru sites. In addition, the oxygen vacancies can enhance the absorption of

DOI: 10.14102/j.cnki.0254-5861.2022-0212

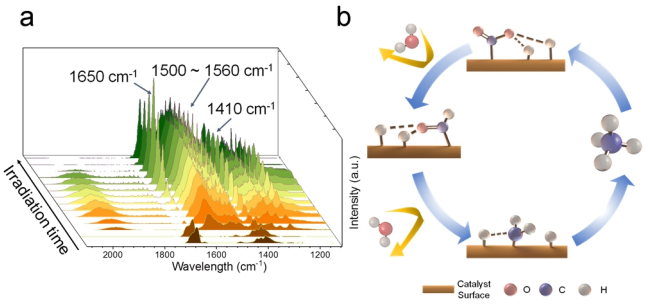

Figure 4. (a) *In situ* DRIFTS spectra during CO_2 methanation reaction. (b) The proposed reaction pathway for the photocatalytic CO_2 methanation reaction.

visible-near infrared light at a range of 400-2000 nm (Figure 2f). Finally, the existence of oxygen vacancies can effectively regulate the loading amount of Ru sites and thus specific surface area of catalysts. So far, two main pathways for CO_2 methanation reaction have been proposed: (1) associative path, where oxygenate intermediates are first produced by reacting CO_2 with H adatom (H_{ad}) species; (2) dissociative path, in which CO_2 is first dissociated to carbonyl and O adatom (O_{ad}) species.[48] To explore the reaction pathway and mechanism in this work, *in situ* diffuse reflectance infrared Fourier transformations spectroscopy (DRIFTS) was therefore performed as shown in Figure 4a. Under CO_2 atmosphere, the two obvious peaks at 1650 and 1410 cm^{-1} corresponding to formate are observed,[49] and the other weak peaks between 1560 and 1500 cm^{-1} corresponding to surface formates are also identified.[50] Notably, the peak at around 2000 cm^{-1} attributed to carbonyl species is not observed, indicating that the carbonyl species produced by dissociative path is not an essential intermediate.[48-56] In addition, the DRIFTS under a CO atmosphere shows the four peaks at 2172, 2115, 2060 and 1960 cm^{-1} are observed, which are assigned as the absorbed CO on the Ru NPs (Figure S14).[50] Thus, it can be inferred that the main reaction pathway is an associative path, as shown in Figure 4b. Briefly, CO_2 and H_2 are firstly adsorbed on the surface of catalyst to produce CO_2 adsorption species and H_{ad} species, respectively. Then the C-O bond is broken and thus the C-H bond is concurrently formed with formate intermediate. Finally, the methane is obtained by further hydrogenation.[48] The proposed photocatalytic CO_2 methanation pathway is different from that of the reported thermocatalytic process.[48-50,52,56]

n CONCLUSIONS

In summary, the Ru-doped TiO_2 photocatalysts with tunable oxygen vacancies have been successfully synthesized by using ascorbic acid as a reducing agent. In a photocatalytic CO_2 methanation reaction, the optimal Ru/TiO_2-OV-50 exhibited a remarkable performance with an 81.7 $mmol \cdot g^{-1} \cdot h^{-1}$ reaction rate and 100% CH_4 selectivity under a 1.5 $W \cdot cm^{-2}$ light illumination, which was much better than that of commercial Ru/TiO_2 and other reported catalysts. The detailed characterizations and experimental results revealed that the highly efficient photocatalytic CO_2 methanation performance was mainly attributed to the synergistic effect of metallic Ru site and TiO_2 with tunable oxygen vacancies. Meanwhile, the CO_2 methanation performance was resulted from the light rather than the thermal effect. Moreover, based on the *in situ* spectroscopic analysis, we proposed the reaction pathway of CO_2 methanation on this photocatalyst. It is hoped that this work would provide new insights for the design and synthesis of efficient photocatalysts for solar-driven CO_2 transformation.

n EXPERIMENTAL

Chemicals

Lithium acetate, ascorbic acid, ruthenium chloride hydrate ($RuCl_3 \cdot xH_2O$) and commercial titanium dioxide (30 nm, anatase) were purchased from Aladdin Biochemical Technology Co., Ltd. N,N-dimethylformamide, acetic acid, tetrabutyl titanate and ammonia solution were purchased from Sinopharm Chemical Reagent Co., Ltd.

Catalysts Preparation

Synthesis of TiO_2-OV-x. The titanium dioxides with tunable oxygen vacancies were synthesized via a simple solvothermal method. Firstly, 200 mg lithium acetate and *x* (*x* = 0, 25, 50, 75 or 100) mg ascorbic acid were successively added into a mixture of 6 mL N,N-dimethylformamide (DMF) and 4 mL acetic acid with continuous stirring until complete dissolution. Subsequently, 2 mL tetrabutyl titanate was added dropwise with stirring, and then the solution was transferred into a 100 mL Teflon-lined autoclave and heated at 200 °C for 20 h. The obtained precipitate was washed with deionized water and ethanol for three times and dried in an oven for 12 hours. The final product was denoted as TiO_2-OV-x.

Synthesis of Ru/TiO_2-OV-x. The Ru-doped titanium dioxides were synthesized by an electrostatic adsorption-reduction method. For a typical synthesis of Ru/TiO_2-OV-50, 100 mg TiO_2-OV-50 was first dissolved in a mixture solution containing 30 mL deionized water and 7.5 mL ammonia. Then, 11.9 mg $RuCl_3 \cdot xH_2O$ was dissolved in another mixture solution containing 3 mL deionized water and 0.75 mL ammonia. After that, two solutions were mixed and stirred for 4 h. The obtained precursor was washed with deionized water and dried in an oven overnight. Subsequently, the precursor powder was reduced at 400 °C for 2 h with a heating rate of 5 °C min^{-1} under a 10 vol% H_2/Ar flow to obtain Ru/TiO_2-OV-50. The other Ru-doped titanium dioxide catalysts (Ru/TiO_2-OV-x) were prepared by the same procedure, except that different titanium dioxides were used.

Catalysts Characterization

Scanning electron microscopy (SEM) images were taken on a ZEISS GeminiSEM 450 Schottky field-emission scanning electron microscope operated at 5 kV. TEM images and the corresponding EDS mapping analysis images were taken on a JEOL JEM-2100 Plus field-emission high-resolution transmission electron microscope operated at 200 kV. Powder XRD patterns were recorded by using a Philips X'Pert Pro Super X-ray diffractometer with Cu-Kα radiation (λ = 1.5418 Å). UV-vis-NIR diffuse reflectance data were recorded in the spectral region of 240-800 nm with a Shimadzu SolidSpec-3700 spectrophotometer. XPS

DOI: 10.14102/j.cnki.0254-5861.2022-0212

was recorded on an X-ray photoelectron spectrometer (Thermo ESCALAB 250, USA). The specific surface areas were determined by BET measurement (JK-BK200C, JWGB SCI. & TECH) using a nitrogen adsorption-desorption isotherm at 77 K. X-ray absorption fine structure (XAFS) measurements were measured at the BL14W1 beamline in Shanghai Synchrotron Radiation Facility and Singapore Synchrotron Light Source. *In situ* DRIFTS measurements were performed using a Bruker IFS 66v Fourier-transform spectrometer equipped with a Harrick diffuse reflectance accessory at the Infrared Spectroscopy and Microspectroscopy Endstation (BL01B) in the NSRL. EPR spectra were collected using a JEOL JES-FA200 electron spin resonance spectrometer at 140 K (9.062 GHz). The Ru contents were measured by ICP-AES. The photocurrent curves and EIS experiments were carried out on a CHI660E electrochemical workstation.

Photocatalytic CO_2 Methanation Measurements

In a typical measurement, 5 mg of catalyst was first dissolved in 300 μL deionized water and dispersed evenly on the surface of a FTO glass slice (15mm × 30mm × 2.2mm). Then the glass slice was placed into a 32 mL custom-made quartz tube. The custom-made photoreactor was continuously degassed and purged with a mixture of CO_2 and H_2 (3:1) three times. After the photoreactor was sealed, the reaction was conducted for 1.5 h under the irradiation of a 300 W Xenon lamp (Beijing Perfectlight, PLS-SXE300D). After reaction, the amounts of CO and CH_4 were determined using a flame ionization detector (FID) of the gas chromatograph (GC, 7890A, Agilent). Other products such as C_2H_4 were determined by another gas chromatograph (GC, 7890B, Agilent) equipped with thermal conductivity detector and flame ionization detector (FID).

n ACKNOWLEDGEMENTS

We acknowledge financial support from the National Key R&D Program of China (2020YFA0406103), NSFC (21725102, 51902311, 22122506, 91961106, 22075267, 22232003), Open Funding Project of National Key Laboratory of Human Factors Engineering (SYFD062010K), Strategic Priority Research Program of the CAS (XDPB14), Anhui Provincial Natural Science Foundation (2008085J05), Youth Innovation Promotion Association of CAS (2019444), Users with Excellence Program of Hefei Science Center CAS (2020HSC-UE003), and Fundamental Research Funds for the Central Universities (WK2060000039). The authors thank the support from USTC Center for Micro- and Nanoscale Research and Fabrication.

n AUTHOR INFORMATION

Corresponding authors. Emails: yjxiong@ustc.edu.cn and wbgong2021@ustc.edu.cn

n AUTHOR CONTRIBUTION

Z.L. and D.W. contribute equally to this work.

n COMPETING INTERESTS

The authors declare no competing interests.

n ADDITIONAL INFORMATION

Supplementary information is available for this paper at http://manu30.magtech.com.cn/jghx/EN/10.14102/j.cnki.0254-5861.2022-0212

For submission: https://www.editorialmanager.com/cjschem

n REFERENCES

(1) Gao, P.; Li, S.; Bu, X.; Dang, S.; Liu, Z.; Wang, H.; Zhong, L.; Qiu, M.; Yang, C.; Cai, J.; Wei, W.; Sun, Y. Direct conversion of CO_2 into liquid fuels with high selectivity over a bifunctional catalyst. *Nat. Chem.* **2017**, 9, 1019-1024.

(2) Wang, L.; Zhang, W.; Zheng, X.; Chen, Y.; Wu, W.; Qiu, J.; Zhao, X.; Zhao, X.; Dai, Y.; Zeng, J. Incorporating nitrogen atoms into cobalt nanosheets as a strategy to boost catalytic activity toward CO_2 hydrogenation. *Nat. Energy* **2017**, 2, 869-876.

(3) Cai, M.; Wu, Z.; Li, Z.; Wang, L.; Sun, W.; Tountas, A. A.; Li, C.; Wang, S.; Feng, K.; Xu, A.-B.; Tang, S.; Tavasoli, A.; Peng, M.; Liu, W.; Helmy, A. S.; He, L.; Ozin, G. A.; Zhang, X. Greenhouse-inspired supra-photothermal CO_2 catalysis. *Nat. Energy* **2021**, 6, 807-814.

(4) Barrio, J.; Mateo, D.; Albero, J.; García, H.; Shalom, M. A heterogeneous carbon nitride-nickel photocatalyst for efficient low-temperature CO_2 methanation. *Adv. Energy Mater.* **2019**, 9, 1902738.

(5) Kattel, S.; Liu, P.; Chen, J. G. Tuning selectivity of CO_2 hydrogenation reactions at the metal/oxide interface. *J. Am. Chem. Soc.* **2017**, 139, 9739-9754.

(6) Guo, Y.; Mei, S.; Yuan, K.; Wang, D.-J.; Liu, H.-C.; Yan, C.-H.; Zhang, Y.-W. Low-temperature CO_2 methanation over CeO_2-supported Ru single atoms, nanoclusters, and nanoparticles competitively tuned by strong metal-support interactions and H-spillover effect. *ACS Catal.* **2018**, 8, 6203-6215.

(7) Wan, L.; Zhou, Q.; Wang, X.; Wood, T. E.; Wang, L.; Duchesne, P. N.; Guo, J.; Yan, X.; Xia, M.; Li, Y. F.; Jelle, A. A.; Ulmer, U.; Jia, J.; Li, T.; Sun, W.; Ozin, G. A. Cu_2O nanocubes with mixed oxidation-state facets for (photo)catalytic hydrogenation of carbon dioxide. *Nat. Catal.* **2019**, 2, 889-898.

(8) Chen, Y.; Zhang, Y.; Fan, G.; Song, L.; Jia, G.; Huang, H.; Ouyang, S.; Ye, J.; Li, Z.; Zou, Z. Cooperative catalysis coupling photo-/photothermal effect to drive Sabatier reaction with unprecedented conversion and selectivity. *Joule* **2021**, 5, 3235-3251.

(9) Han, S.; Li, B.; Huang, L.; Xi, H.; Ding, Z.; Long, J. Construction of $ZnIn_2S_4$-$CdIn_2S_4$ microspheres for efficient photo-catalytic reduction of CO_2 with visible light. *Chin. J. Struct. Chem.* **2022**, 41, 2201007-2201013.

(10) Wang, Z.; Hong, J.; Ng, S.-F.; Liu, W.; Huang, J.; Chen, P.; Ong, W.-J. Recent progress of perovskite oxide in emerging photocatalysis landscape: water splitting, CO_2 reduction, and N_2 fixation. *Acta Phys. Chim. Sin.* **2021**, 37, 2011033.

(11) Li, N.; Peng, J.; Shi, Z.; Zhang, P.; Li, X. Charge transfer and orbital reconstruction of non-noble transition metal single-atoms anchored on Ti_2CT_x-MXenes for highly selective CO_2 electrochemical reduction. *Chin. J. Catal.* **2022**, 43, 1906-1917.

(12) Xu, Z.-T., X.; Xie, K. Enhanced CO_2 electrolysis with metal-oxide interface structures. *Chin. J. Struct. Chem.* **2021**, 40, 31-41.

(13) Wang, C.; Sun, Z.; Zheng, Y.; Hu, Y. H. Recent progress in visible light photocatalytic conversion of carbon dioxide. *J. Mater. Chem. A* **2019**, 7, 865-887.

(14) He, K.; Shen, R.; Hao, L.; Li, Y.; Zhang, P.; Jiang, J.; Xin, L. Advances in nanostructured silicon carbide photocatalysts. *Acta Phys. Chim. Sin.* **2022**, 38, 2201021.

(15) Chai, Y.; Chen, Y.; Wang, B.; Jiang, J.; Liu, Y.; Shen, J.; Wang, X.; Zhang, Z. Sn^{2+} and Cu^{2+} self-codoped Cu_2ZnSnS_4 nanosheets switching from p-type to n-type semiconductors for visible-light-driven CO_2 reduction. *ACS Sustain.*

DOI: 10.14102/j.cnki.0254-5861.2022-0212

Chem. Eng. **2022**, 10, 8825-8834.
(16) Shen, R.; Hao, L.; Ng, Y. H.; Zhang, P.; Arramel, A.; Li, Y.; Li, X. Heterogeneous N-coordinated single-atom photocatalysts and electrocatalysts. *Chin. J. Catal.* **2022**, 43, 2453-2483.
(17) Quan, F.; Zhan, G.; Mao, C.; Ai, Z.; Jia, F.; Zhang, L.; Gu, H.; Liu, S. Efficient light-driven CO_2 hydrogenation on Ru/CeO_2 catalysts. *Catal. Sci. Technol.* **2018**, 8, 6503-6510.
(18) Lin, L.; Wang, K.; Yang, K.; Chen, X.; Fu, X.; Dai, W. The visible-light-assisted thermocatalytic methanation of CO_2 over $Ru/TiO_{(2-x)}N_x$. *Appl. Catal., B.* **2017**, 204, 440-455.
(19) Mateo, D.; Albero, J.; Garcia, H. Titanium-perovskite-supported RuO_2 nanoparticles for photocatalytic CO_2 methanation. *Joule* **2019**, 3, 1949-1962.
(20) Sun, Z.; Talreja, N.; Tao, H.; Texter, J.; Muhler, M.; Strunk, J.; Chen, J. Catalysis of carbon dioxide photoreduction on nanosheets: fundamentals and challenges. *Angew. Chem. Int. Ed.* **2018**, 57, 7610-7627.
(21) Zhou, Y.; Zhang, Q.; Shi, X.; Song, Q.; Zhou, C.; Jiang, D. Photocatalytic reduction of CO_2 into CH_4 over Ru-doped TiO_2: synergy of Ru and oxygen vacancies. *J. Colloid Interf. Sci.* **2022**, 608, 2809-2819.
(22) Liu, Y.; Yu, F.; Wang, F.; Bai, S.; He, G. Construction of Z-scheme In_2S_3-TiO_2 for CO_2 reduction under concentrated natural sunlight. *Chin. J. Struct. Chem.* **2022**, 41, 2201034-2201039.
(23) Su, B.; Huang, H.; Ding, Z.; Roeffaers, M. B. J.; Wang, S.; Long, J. S-scheme $CoTiO_3/Cd_{9.51}Zn_{0.49}S_{10}$ heterostructures for visible-light driven photocatalytic CO_2 reduction. *J. Mater. Sci. Technol.* **2022**, 124, 164-170.
(24) Wu, Z.; Guo, S.; Kong, L.-H.; Geng, A.-F.; Wang, Y.-J.; Wang, P.; Yao, S.; Chen, K.-K.; Zhang, Z.-M. Doping $[Ru(bpy)_3]^{2+}$ into metal-organic framework to facilitate the separation and reuse of noble-metal photosensitizer during CO_2 photoreduction. *Chin. J. Catal.* **2021**, 42, 1790-1797.
(25) Chai, S.; Men, Y.; Wang, J.; Liu, S.; Song, Q.; An, W.; Kolb, G. Boosting CO_2 methanation activity on Ru/TiO_2 catalysts by exposing (001) facets of anatase TiO_2. *J. CO_2 Util.* **2019**, 33, 242-252.
(26) Abe, T.; Tanizawa, M.; Watanabe, K.; Taguchi, A. CO_2 methanation property of Ru nanoparticle-loaded TiO_2 prepared by a polygonal barrel-sputtering method. *Energy Environ. Sci.* **2009**, 2, 315-321.
(27) Kar, P.; Farsinezhad, S.; Mahdi, N.; Zhang, Y.; Obuekwe, U.; Sharma, H.; Shen, J.; Semagina, N.; Shankar, K. Enhanced CH_4 yield by photocatalytic CO_2 reduction using TiO_2 nanotube arrays grafted with Au, Ru, and ZnPd nanoparticles. *Nano Res.* **2016**, 9, 3478-3493.
(28) Li, X.; Yu, J.; Jaroniec, M.; Chen, X. Cocatalysts for selective photoreduction of CO_2 into solar fuels. *Chem. Rev.* **2019**, 119, 3962-4179.
(29) Liu, S.; Li, Y.; Ding, K.; Chen, W.; Zhang, Y.; Lin, W. Mechanism on carbon vacancies in polymeric carbon nitride for CO_2 photoreduction. *Chin. J. Struct. Chem.* **2020**, 39, 2068-2076.
(30) Wang, R.; Yang, P.; Wang, S.; Wang, X. Distorted carbon nitride nanosheets with activated n→π* transition and preferred textural properties for photocatalytic CO_2 reduction. *J. Catal.* **2021**, 402, 166-176.
(31) Li, D.; Huang, Y.; Li, S.; Wang, C.; Li, Y.; Zhang, X.; Liu, Y. Thermal coupled photoconductivity as a tool to understand the photothermal catalytic reduction of CO_2. *Chin. J. Catal.* **2020**, 41, 154-160.
(32) Zhou, J.; Gao, Z.; Xiang, G.; Zhai, T.; Liu, Z.; Zhao, W.; Liang, X.; Wang, L. Interfacial compatibility critically controls Ru/TiO_2 metal-support interaction modes in CO_2 hydrogenation. *Nat. Commun.* **2022**, 13, 327.
(33) Panagiotopoulou, P. Methanation of CO_2 over alkali-promoted Ru/TiO_2 catalysts: II. Effect of alkali additives on the reaction pathway. *Appl. Catal., B* **2018**, 236, 162-170.
(34) Li, M.; Li, P.; Chang, K.; Wang, T.; Liu, L.; Kang, Q.; Ouyang, S.; Ye, J. Highly efficient and stable photocatalytic reduction of CO_2 to CH_4 over Ru loaded $NaTaO_3$. *Chem. Commun.* **2015**, 51, 7645-7648.
(35) Cai, S.; Zhang, M.; Li, J.; Chen, J.; Jia, H. Anchoring single-atom Ru on CdS with enhanced CO_2 capture and charge accumulation for high selectivity of photothermocatalytic CO_2 reduction to solar fuels. *Solar RRL* **2021**, 5, 2000313.
(36) Lin, Y.; Tian, Z.; Zhang, L.; Ma, J.; Jiang, Z.; Deibert, B. J.; Ge, R.; Chen, L. Chromium-ruthenium oxide solid solution electrocatalyst for highly efficient oxygen evolution reaction in acidic media. *Nat. Commun.* **2019**, 10, 162.
(37) Jarzembska, K.; Seal, S.; Woźniak, K.; Szadkowska, A.; Bieniek, M.; Grela, K. X-ray photoelectron spectroscopy and reactivity studies of a series of ruthenium catalysts. *ChemCatChem* **2009**, 1, 144-151.
(38) Morgan, D. J. Resolving ruthenium: XPS studies of common ruthenium materials. *Surf. Interf. Anal.* **2015**, 47, 1072-1079.
(39) Marchal, C.; Cottineau, T.; Méndez-Medrano, M. G.; Colbeau-Justin, C.; Caps, V.; Keller, V. Au/TiO_2-gC_3N_4 nanocomposites for enhanced photocatalytic H_2 production from water under visible light irradiation with very low quantities of sacrificial agents. *Adv. Energy Mater.* **2018**, 8, 1702142.
(40) Wu, M.; Zhang, J.; Liu, C.; Gong, Y.; Wang, R.; He, B.; Wang, H. Rational design and fabrication of noble-metal-free Ni_xP cocatalyst embedded 3D N-TiO_2/g-C_3N_4 heterojunctions with enhanced photocatalytic hydrogen evolution. *ChemCatChem* **2018**, 10, 3069-3077.
(41) Eom, J.-Y.; Lim, S.-J.; Lee, S.-M.; Ryu, W.-H.; Kwon, H.-S. Black titanium oxide nanoarray electrodes for high rate Li-ion microbatteries. *J. Mater. Chem. A* **2015**, 3, 11183-11188.
(42) Ge, H.; Zhang, B.; Liang, H.; Zhang, M.; Fang, K.; Chen, Y.; Qin, Y. Photocatalytic conversion of CO_2 into light olefins over TiO_2 nanotube confined Cu clusters with high ratio of Cu^+. *Appl. Catal., B* **2020**, 263, 118133.
(43) Yin, G.; Huang, X.; Chen, T.; Zhao, W.; Bi, Q.; Xu, J.; Han, Y.; Huang, F. Hydrogenated blue titania for efficient solar to chemical conversions: preparation, characterization, and reaction mechanism of CO_2 reduction. *ACS Catal.* **2018**, 8, 1009-1017.
(44) Zhou, Z.; Li, X.; Li, J.; You, Z. Promoting CO_2 methanation performance of Ru/TiO_2 through Co-activity of exposing (001) facets and oxygen vacancies of TiO_2. *Mater. Sci. Semicon. Proc.* **2022**, 146, 106677.
(45) Cheng, S.; Gao, Y.-J.; Yan, Y.-L.; Gao, X.; Zhang, S.-H.; Zhuang, G.-L.; Deng, S.-W.; Wei, Z.-Z.; Zhong, X.; Wang, J.-G. Oxygen vacancy enhancing mechanism of nitrogen reduction reaction property in Ru/TiO_2. *J. Energy Chem.* **2019**, 39, 144-151.
(46) Chen, S.; Abdel-Mageed, A. M.; Li, D.; Bansmann, J.; Cisneros, S.; Biskupek, J.; Huang, W.; Behm, R. J. Morphology-engineered highly active and stable Ru/TiO_2 catalysts for selective CO methanation. *Angew. Chem. Int. Ed.* **2019**, 58, 10732-10736.
(47) Du, J.; Huang, Y.; Huang, Z.; Wu, G.; Wu, B.; Han, X.; Chen, C.; Zheng, X.; Cui, P.; Wu, Y. Reversing the catalytic selectivity of single-atom Ru via support amorphization. *JACS Au* **2022**, 2, 1078-1083.
(48) Miao, B.; Ma, S. S. K.; Wang, X.; Su, H.; Chan, S. H. Catalysis mechanisms of CO_2 and CO methanation. *Catal. Sci. Technol.* **2016**, 6, 4048-4058.
(49) Gupta, N.; Kamble, V.; Kartha, V.; Iyer, R.; Thampi, K. R.; Gratzel, M. FTIR spectroscopic study of the interaction of CO_2 and CO_2 + H_2 over partially oxidized $RuTiO_2$ catalyst. *J. Catal.* **1994**, 146, 173-184.
(50) Abdel-Mageed, A. M.; Widmann, D.; Olesen, S. E.; Chorkendorff, I.; Biskupek, J.; Behm, R. J. Selective CO methanation on Ru/TiO_2 catalysts: role and influence of metal-support interactions. *ACS Catal.* **2015**, 5, 6753-6763.
(51) Aldana, P. A. U.; Ocampo, F.; Kobl, K.; Louis, B.; Thibault-Starzyk, F.; Daturi, M.; Bazin, P.; Thomas, S.; Roger, A. C. Catalytic CO_2 valorization into CH_4 on Ni-based ceria-zirconia. Reaction mechanism by operando IR

DOI: 10.14102/j.cnki.0254-5861.2022-0212

spectroscopy. *Catal. Today* **2013**, 215, 201-207.

(52) Dalla Betta, R.; Shelef, M. Heterogeneous methanation: in situ infrared spectroscopic study of $RuAl_2O_3$ during the hydrogenation of CO. *J. Catal.* **1977**, 48, 111-119.

(53) Eckle, S.; Anfang, H.-G.; Behm, R. J. R. Reaction intermediates and side products in the methanation of CO and CO_2 over supported Ru catalysts in H_2-rich reformate gases. *J. Phys. Chem. C* **2011**, 115, 1361-1367.

(54) Eckle, S.; Denkwitz, Y.; Behm, R. J. Activity, selectivity, and adsorbed reaction intermediates/reaction side products in the selective methanation of CO in reformate gases on supported Ru catalysts. *J. Catal.* **2010**, 269, 255-268.

(55) Prairie, M. R.; Renken, A.; Highfield, J. G.; Thampi, K. R.; Grätzel, M. A fourier transform infrared spectroscopic study of CO_2 methanation on supported ruthenium. *J. Catal.* **1991**, 129, 130-144.

(56) Zhang, S.-T.; Yan, H.; Wei, M.; Evans, D. G.; Duan, X. Hydrogenation mechanism of carbon dioxide and carbon monoxide on Ru(0001) surface: a density functional theory study. *RSC Adv.* **2014**, 4, 30241-30249.

Received: October 22, 2022
Accepted: November 11, 2022
Published online: November 16, 2022
Published: December 2, 2022

DOI: 10.14102/j.cnki.0254-5861.2022-0212